JOC The Journal of Organic Chemistry

Article

pubs.acs.org/joc

Switching of the Triplet Excited State of Rhodamine/Naphthaleneimide Dyads: An Experimental and Theoretical Study

Xiaoneng Cui,[†] Jianzhang Zhao,*[,†] Zhangrong Lou,[†] Shujing Li,[‡] Huijian Wu,*[,‡] and Ke-li Han*[,§]

[†]State Key Laboratory of Fine Chemicals, School of Chemical Engineering and [‡]School of Life Science and Biotechnology, Dalian University of Technology, Dalian 116024, China

[§]State Key Laboratory of Molecular Reaction Dynamics, Dalian Institute of Chemical Physics (DICP), Chinese Academy of Sciences (CAS), Dalian 116023, P. R. China

Supporting Information

ABSTRACT: Rhodamine−bromonaphthaleneimide (**RB−NI**) and rhodamine−bromonaphthalenediimide (**RB−NDI**) dyads were prepared for switching of the *triplet* excited states. Bromo-NI or bromo-NDI parts in the dyads are the spin converters, i.e., the triplet state producing modules, whereas the RB unit is the acid-activatable electron donor/energy acceptor. NI and NDI absorb at 359 and 541 nm, and the T_1 state energy levels are 2.25 and 1.64 eV, respectively. RB undertakes the reversible spirolactam (RB-c) ↔ opened amide (RB-o) transformation. RB-c shows no visible light absorption, and the triplet-state energy level is E_{T1} = 3.36 eV. Conversely RB-o shows strong absorption at 557 nm, and E_{T1} is 1.73 eV. Thus, the acid-activated fluorescence-resonance-energy-transfer (FRET) competes with the ISC of NI or NDI. No triplet state was observed for the dyads with nanosecond time-resolved transient absorption spectroscopy. Upon addition of acid, strong fluorescence and long-living triplet excited states were observed. Thus, the producing of triplet state is acid-activatable. The triplet state of **RB−NI** is *localized* on RB-o part, whereas in **RB−NDI** the triplet state is *delocalized* on both the NDI and RB-o units. The ISC of spin converter was not outcompeted by RET. These studies are useful for switching of triplet excited state.

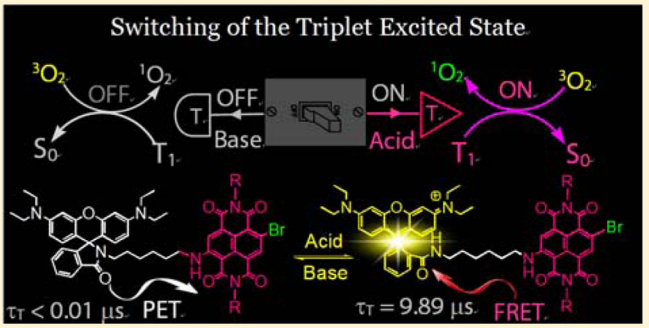

1. INTRODUCTION

Triplet photosensitizers are versatile compounds and have been widely used in photodynamic therapy,[1−8] photocatalysis,[9] molecular logic gates,[10] as well as in studies of photochemistry and photophysics.[11−14] However, *switching* of the *triplet* excited state was rarely studied,[10,15] which is in stark contrast to the study of *singlet* excited states. Various mechanisms have been developed for controlling singlet excited state of fluorophores (mainly related to fluorescence).[16] For example, the emission from singlet excited state of organic chromophores can be readily turned ON or OFF by controlling the photoinduced electron transfer (PET),[16] photoinduced intramolecular charge transfer (ICT), and fluorescence resonance energy transfer (FRET) or through-bond-energy-transfer (TBET).[16−18] On the basis of these mechanisms, many functional compounds have been developed, such as fluorescent molecular probes, molecular logic gates, and light-harvesting molecular arrays, etc.[16−21]

Intramolecular triplet energy transfer between naphthalene and benzophenone has been studied.[22] Based on the development of production of triplet excited states,[8] we envisage the next logic step will be to switch the triplet states. Concerning this aspect, controlling *triplet* excited state will be significant in many areas, such as pH- or enzyme-activatable PDT reagents,[3] molecular logic gates,[10] and study of the fundamental photochemistry of organic chromophores. However, such investigations were rarely reported. Previously photochromic units such as dithienylethene (DTE) have been used for preparation of Ru(II), Os(II), and Ir(III) complexes.[23,24] Recently, Bodipy dyads were studied as molecular logic gates, for which the singlet oxygen ($^1O_2$) photosensitizing ability was changed by addition of acid/base, via controlling the direction of FRET.[10,15] Unfortunately, the switching of *triplet* states in organic compounds has not been studied in detail, such as with the nanosecond time-resolved transient difference absorption spectroscopy.[10,15,25] Moreover, the mechanisms for triplet-state controll are very limited. Thus, in comparison with the development of the *singlet* excited state switching,[16] the study on *triplet* excited state switching is still in its infancy.

In order to address the above challenges, herein we prepared rhodamine−naphthaleneimide (**RB−NI**) and rhodamine−naphthalenediimide (**RB−NDI**) dyads to investigate the switching of the triplet excited state with external stimuli such as acid/base. Rhodamine is well-known for the acid/base-promoted spirolactam (RB-c) ↔ opened amide (RB-o) reversible transformation.[17,26−29] The photophysical changes companying the structure transformation are the turn-ON and

Received: November 8, 2014
Published: December 1, 2014

   dx.doi.org/10.1021/jo502554y | J. Org. Chem. 2015, 80, 568−581

Scheme 1. Synthesis of the Acid/Base Switchable Dyads RB−NI and RB−NDI[a]

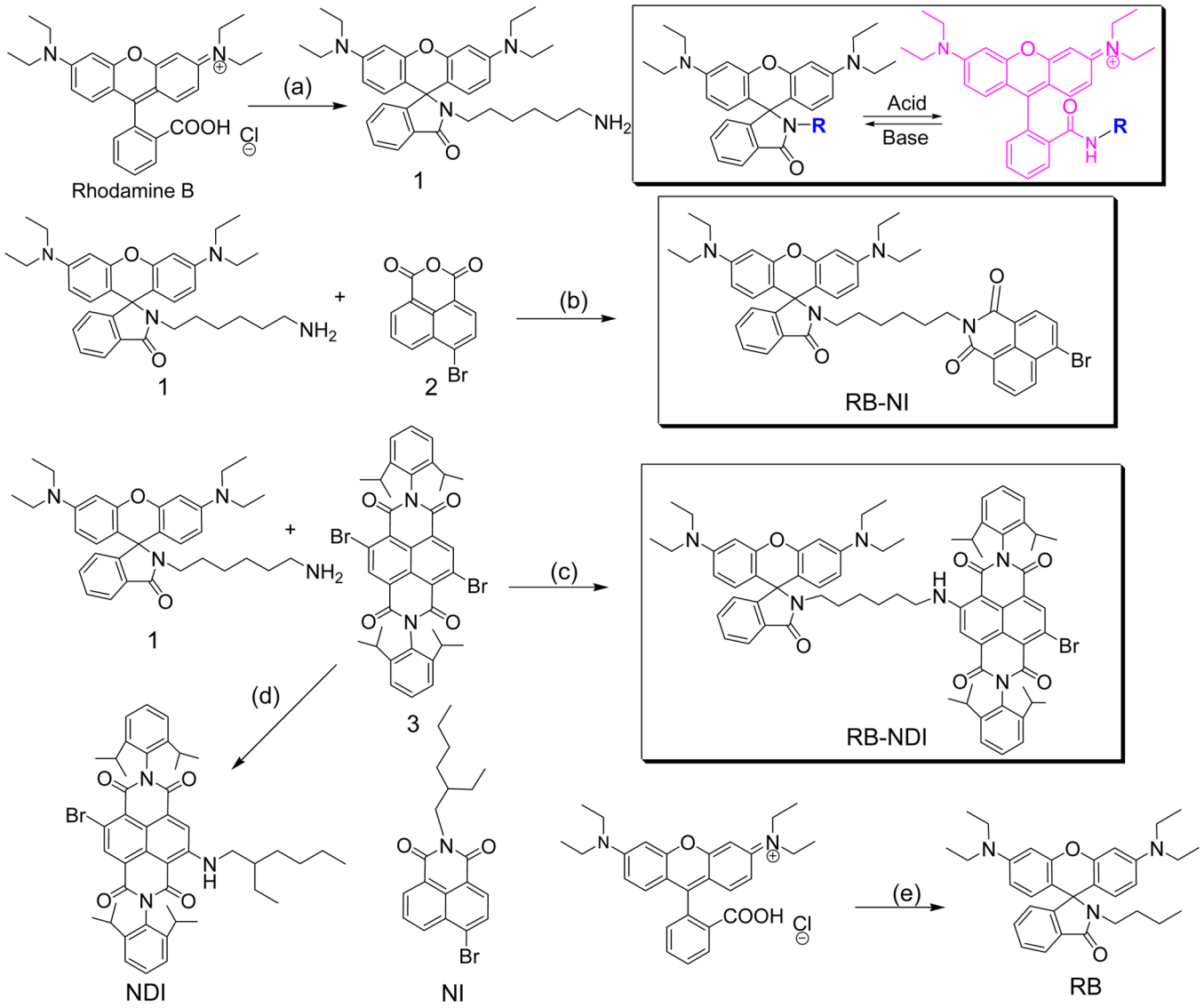

[a]Key: (a) under Ar, 1,6-hexanediamine, EtOH, 120 °C, reflux, 12 h; yield 88%; (b) under Ar, EtOH, 80 °C, reflux, 8 h; yield 83%; (c) under Ar, 2-methoxyethanol, 120 °C, reflux, 8 h; yield 33%; (d) 2-ethylhexylamine, 2-methoxyethanol, 120 °C, 8 h, yield 54%; (e) under Ar, *n*-butylamine, EtOH, 120 °C, reflux, 8 h; yield 87%. The known compounds **3** and **NI** were presented.

-OFF of the absorption band at ca. 557 nm, as well as the fluorescence at 580 nm (S_1 state for rhodamine B).[28]

With the reversible spirolactam ↔ opened amide switching of rhodamine, the π-conjugation framework of the rhodamine moiety undergoes substantial change; thus, we postulate that the T_1 state energy level of rhodamine will change as well. However, this approach has never been used for *triplet* excited state switching. In **RB−NI** and **RB−NDI** (Scheme 1), the NI and NDI units have bromo substituents; thus, these modules are able to produce triplet excited state upon photoexcitation; i.e., these Br-containing moieties act as "intramolecular spin converters".[8,13,14,30−32] Rhodamine B was reported with a T_1 state energy level (E_{T1}) of ca. 1.74 eV.[33] For the NDI moiety, E_{T1} is ca. 1.58 eV. NI gives E_{T1} of 2.07 eV. Thus, we postulate that the triplet excited state property of the dyads **RB−NI** and **RB−NDI**, in the aspects of yield, lifetime, and spatical localization, may be controlled by the acid/based activated cyclic lactam ↔ open amide transformation of the rhodamine subunits, thus the controllable FRET and the triplet-state energy-transfer effect.[10]

The photophysical properties of the dyads were studied in detail with steady-state and nanosecond time-resolved transient absorption spectroscopy, as well as DFT/TDDFT computations. We found that the *triplet* excited-state properties of the dyads can be switched-ON with acid and switched-OFF with base. DFT/TDDFT calculations rationalized the experimental observations. The results prove that the RET failed to inhibit the intersystem crossing (ISC) of the spin converters in the dyads.[10] Instead, the acid-modulated intramolecular electron transfer plays a decisive role on the production of triplet states. The acid/base modulation of the triplet-state production of the dyads was transduced to the $^1O_2$ photosensitizing ability. These investigations shed light on the photochemistry of the dyad organic *triplet* photosensitizers, and it will be helpful for designing of external stimuli-activatable triplet state-based functional molecular assemblies.[10,15]

dx.doi.org/10.1021/jo502554y | *J. Org. Chem.* 2015, 80, 568−581

2. RESULTS AND DISCUSSION

2.1. Design and Synthesis of the Dyads. In dyads **RB−NI** and **RB−NDI** (Scheme 1), bromo-NI and bromo-NDI modules were used as intramolecular spin converters to produce the triplet state via ISC upon photoexcitation.[8,34,35] On the contrary, ISC is very weak for the rhodamine unit alone.[36] In **RB−NI** and **RB−NDI**, the absorption band of RB-o overlaps with the emission band of NI or NDI moiety. Thus, singlet resonance energy transfer (RET) from the bromo-NI or the bromo-NDI to the RB-o will compete with the ISC of NI or NDI modules.[10,28] For **RB−NI** and **RB−NDI** with RB units in the spirolactam structure, no such RET exists. Competition of RET with ISC of NI/NDI can be evaluated by the triplet state yields of the dyads. Given the ISC was overwhelmingly outcompeted by the RET, then no triplet excited state should be observed for the dyads upon photoexcitation into the singlet energy donor (NI or NDI modules). Moreover, it was reported that the triplet state energy level of rhodamine B is ca. 1.74 eV.[33] The NI moiety gives the T_1 state energy level as 2.07 eV. Therefore, the localization of the triplet state of **RB−NI** may shift from the NI moiety to the RB-o part upon addition of acid. For **RB−NDI**, however, the NDI part is with E_{T1} at 1.65 eV; thus, triplet-state equilibrium between NDI and RB-o moiety may be established. Interestingly, our study shows that the switching of the triplet state does not strictly follow the above postulation; instead, the intramolecular electron transfer from the RB(c) to the NI or NDI moiety dictates the production of the triplet excited states.

The two chromophores in **RB−NI** and **RB−NDI** were connected by a flexible 1,6-hexyldiamine linker (Scheme 1); thus the triplet energy transfer (very often via Dexter mechanism, contact between the triplet energy donor and acceptor is required, which is different from the dipole interaction of the FRET effect of the *singlet* energy transfer) between the two intramolecular components will be ensured. The rigid linker may hamper the triplet energy transfer.[37]

Reaction of 1,6-hexanediamine with rhodamine B gives the synthon **1** as a white solid because rhodamine moiety is in the spirolactam form. Then reaction of compound **1** with 4-bromo-1,8-naphthalic anhydride (**2**) gives **RB−NI** as a light yellow solid. Synthesis of **RB−NDI** proceeds via a similar method. The two components were linked together with substitution of one bromo atom on NDI, whereas one bromo substituent is retained to ensure ISC.[34,35] Compounds **RB**, **NI**, and **NDI** were prepared as reference for study of the photophysical properties (Scheme 1). In these compounds, the rhodamine unit is in lactam form. All of the compounds were obtained with moderate to satisfactory yields.

2.2. UV−vis Absorption and Fluorescence Emission Spectra. The UV−vis absorption of the dyads **RB−NI** and **RB−NDI** was studied (Figure 1). For **RB−NI**, the absorption maxima is at 356 nm, and no absorption in visible spectral region was observed (Figure 1a). Upon addition of trifluoroacetic acid (TFA), a strong absorption band at 557 nm developed, which is attributed to RB-o. The absorption band can be decreased by addition of base such as triethylamine (TEA).

Thus, the absorption of **RB−NI** in the visible region can be switched ON and OFF by the spirolactam ↔ opened amide transformation of the rhodamine moiety. Similar results were observed for **RB−NDI** (Figure 1b). Different from **RB−NI**, **RB−NDI** shows a moderate absorption band at 537 nm in the absence of TFA, which is due to the NDI moiety.[34,35,38,39] The absorption band of RB-o overlaps with the fluorescence of NDI unit (see later discussion); thus, the RB-o unit can act as the singlet energy acceptor of the RET process in **RB−NI** and **RB−NDI**.

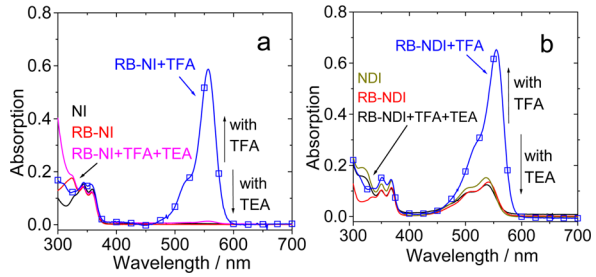

Figure 1. UV−vis absorption spectra of the compounds (a) **RB−NI** and (b) **RB−NDI** in dichloromethane (DCM)/CH_3OH (9:1, v/v). With addition of TFA (5.0 mol/L, 50 μL) or TEA (neat, 50 μL) for the switching purpose. $c = 1.0 \times 10^{-5}$ M. 20 °C.

The fluorescence emission of **NDI** and **RB−NDI** were compared (Figure 2a), upon photoexcitation at a wavelength where the solution of both compounds give same optical density.

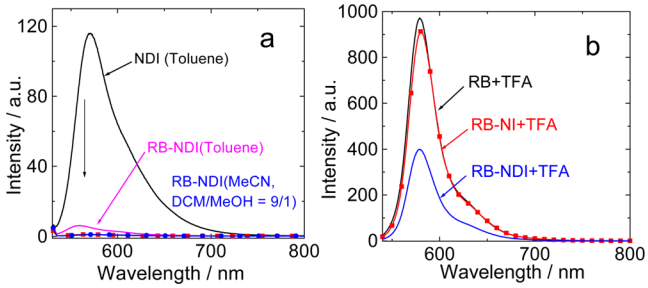

Figure 2. Fluorescence emission spectra of (a) **RB−NDI** and **NDI** (λ_{ex} = 530 nm, at which both solution give same absorbance) and (b) **RB+TFA**, **RB−NI+TFA**, and **RB−NDI+TFA** (λ_{ex} = 530 nm, at which the three samples **RB+TFA**, **RB−NI+TFA**, and **RB−NDI+TFA** give same absorbance) with TFA (5.0 mol/L, 50 μL) added (in DCM/CH_3OH, 9:1, v/v). 20 °C.

Compared with the reference compound **NDI**, the emission of the NDI moiety in **RB−NDI** is drastically quenched (in toluene, Figure 2a). Note that no emission of RB-c should be observed. In a polar solvent such as DCM/MeOH (9/1, v/v), the emission band of NDI can be quenched further (Figure 2a). The quenching of NDI emission in **RB−NDI** is most likely due to the photoinduced electron transfer from the RB-c to the NDI part.[40,41] The electrochemical data, the time-resolved absorption and emission data, and the DFT calculations support electron transfer in **RB−NDI** (see later discussion).

The fluorescence emission intensity of **RB−NI** and **RB−NI** in the presence of TFA were also compared (Figure 2b). For **RB−NI**, no quenching effect of the RB-o emission was observed, indicating no photoinduced electron transfer exists. For **RB−NDI**, however, the fluorescence in the presence of TFA is much weaker than that of RB in the presence of TFA, which may be due to intramolecular electron transfer (the Gibbs free energy change for the electron transfer of **RB−NDI +TFA** was calculated as −0.4 eV, see later discussion).

The reversible switching of fluorescence emission of the dyads upon addition of acid and base was investigated (Figure

dx.doi.org/10.1021/jo502554y | J. Org. Chem. 2015, 80, 568−581

3). Compared with **RB−NI**, **RB−NI+TFA** shows a distinct emission band at 580 nm, which is due to the RB-o part.[28] This

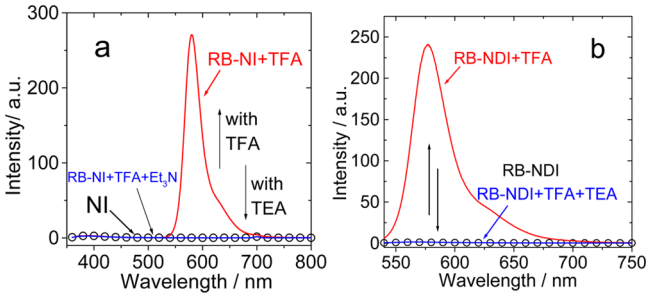

Figure 3. Switching of the fluorescence emission spectra of the dyads with acid (TFA) and base (TEA). (a) Fluorescence of **RB−NI** and **NI** (λ_{ex} = 350 nm) with TFA (5.0 mol/L, 50 μL, standed for 25 min before measurement) and TEA (50 μL, neat) added. (b) Fluorescence emission spectra of **RB−NDI** (λ_{ex} = 530 nm) with TFA (5.0 mol/L, 50 μL, stands for 25 min before measurement) or TEA (50 μL, neat) added. In DCM/CH_3OH (9:1, v/v). $c = 1.0 \times 10^{-5}$ M. 20 °C.

band can be switched OFF by addition of base such as TEA (Figure 3a). Emission of the NI part in **RB−NI** is weak and cannot be discerned in the spectrum. Similar results were found for **RB−NDI** (Figure 3b). Upon addition of TFA, an intense emission band at 580 nm was observed. The emission can be turned off by addition of base such as TEA. NDI alone does not show such a switching effect (see Figure S21, Supporting Information). Thus, the emission of **RB−NDI** in the presence of TFA is due to the RB-o moiety.

Since the emission band of **NDI** is centered at similar wavelength to that of rhodamine, the emission of the related compounds were compared to prove the emission of **RB−NDI** is due to the rhodamine moiety, not the NDI moiety (Figure 4). The emission feature of **RB−NDI+TFA** is in full agreement

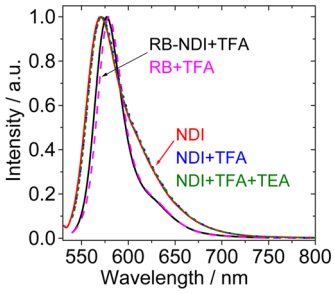

Figure 4. Normalized fluorescence emission spectra of **NDI**, **RB**, and **RB−NDI** (λ_{ex} = 530 nm) with TFA added (5.0 mol/L, 50 μL) and TEA (50 μL, neat) added. In mixed solvent DCM/CH_3OH (9:1, v/v). $c = 1.0 \times 10^{-5}$ M. 20 °C.

with the reference compound **RB** (Scheme 1) in the aspects of both the band shape and the emission wavelength, and it is different from the emission feature of NDI. Thus, we can conclude that the emission of **RB−NDI+TFA** is due to the rhodamine part, not the NDI part.

We noted that the spirolactam → open amide transformation of the RB moiety in the dyads is slow. Although rhodamine has been intensively used in fluorescent molecular sensors by exploring the closed lactam ↔ open amide form transformation,[17,26,28] the reaction kinetics was rarely reported.[17,42] The kinetics is important for applications based on the RB-c/RB-o transformations. The absorption variation of the dyads at 557 nm upon addition of acid were studied (Figure 5). Slow

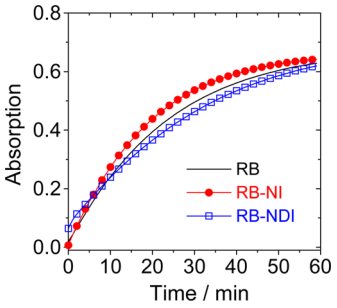

Figure 5. Kinetics of the spirolactam → opened amide transformation of the rhodamine moiety, monitored by following the absorption at 557 nm upon addition of TFA (5.0 mol/L, 50 μL) of compounds **RB**, **RB−NI**, and **RB−NDI**. In DCM/CH_3OH (9:1, v/v). $c = 1.0 \times 10^{-5}$ M. 20 °C.

kinetics were observed for all the rhodamine-containing compounds, with typical rate constants of $k = (4.15 \pm 0.02) \times 10^{-2}$ min^{-1} (for reference compound **RB**) under the experimental conditions. For **RB−NI** and **RB−NDI**, the transformation rate constants are $k = (5.18 \pm 0.02) \times 10^{-2}$ min^{-1} and $k = (2.91 \pm 0.02) \times 10^{-2}$ min^{-1}, respectively. On the basis of these results, sufficient standing time was used in all the measurements in this paper. Interestingly, the reverse open amide → the cyclic lactam transformation of the RB moiety is much faster upon addition of based such as TEA and a few seconds are sufficient.

2.3. Switching of the Triplet Excited State: Nanosecond Time-Resolved Transient Difference Absorption Spectroscopy. In order to study the switching of the triplet excited states of the dyads upon addition of acid or base, nanosecond time-resolved transient difference absorption (TA) spectra were studied (Figure 6). For **NI**, a weak bleaching band at 353 nm was observed upon pulsed laser excitation at 355 nm, which is in agreement with the steady-state absorption of NI moiety. Strong positive absorption bands in the 400−550 nm region were found. The triplet excited-state lifetime was determined as τ_T = 75.2 μs. In the presence of TFA, a similar transient profile was observed (see the Supporting Information, Figure S23, τ_T = 76.6 μs) (Table 1).

For **RB−NI**, however, no transient signal can be detected (the time-resolution limit of the spectrometer is 10 ns). The triplet excited state of NI is presumably quenched by electron transfer.[14] Upon addition of TFA, however, a bleaching band at 553 nm was observed for **RB−NI** upon pulsed laser excitation (Figure 6c), which is due to the steady-state bleaching of the RB-o unit in **RB−NI**. The transient absorption feature is drastically different from that of **NI** (Figure 6a). Thus, we propose the triplet state of **RB−NI** in the presence of TFA is localized on the rhodamine part. The DFT calculations support this assignment (see later discussion).

The nanosecond TA spectra of **NDI** was studied (Figure 7a). Weak bleaching bands at 368 and 541 nm were observed, which is due to the depletion of the ground state of **NDI**. The transient absorption bands centered at 450 nm and in the region of 600−700 nm were observed. The lifetime of the transient signals were determined as 113.5 μs (Figure 7b).[35] The lifetime was significantly reduced to 0.70 μs in aerated solution (see the Supporting Information, Figure S27).

dx.doi.org/10.1021/jo502554y | J. Org. Chem. 2015, 80, 568−581

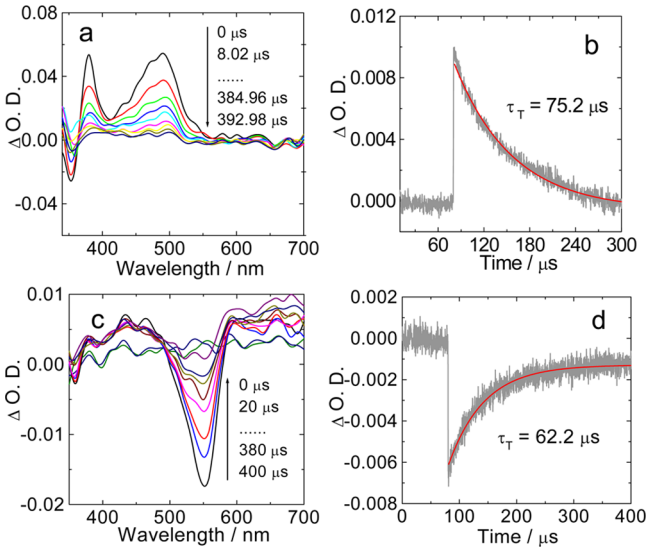

Figure 6. Switching the triplet state of **RB−NI** by addition of TFA, studied by nanosecond time-resolved transient difference absorption spectroscopy. (a) **NI**, $c = 5.0 \times 10^{-5}$ M. (b) Decay trace of **NI** at 480 nm. Excited with 355 nm nanosecond pulsed laser. $c = 1.0 \times 10^{-5}$ M. (c) Transient absorption spectra of **RB−NI** in the presence of TFA (100 μL). $c = 2.0 \times 10^{-5}$ M. (d) Decay trace at 560 nm. $c = 1.0 \times 10^{-5}$ M. Excited with 355 nm nanosecond pulsed laser excitation. In deaerated DCM/MeOH (9/1, v/v). 20 °C. To optimize the signal/noise ratio in the spectra and to avoid triplet−triplet annihilation effect, different concentration were used in the measurements.

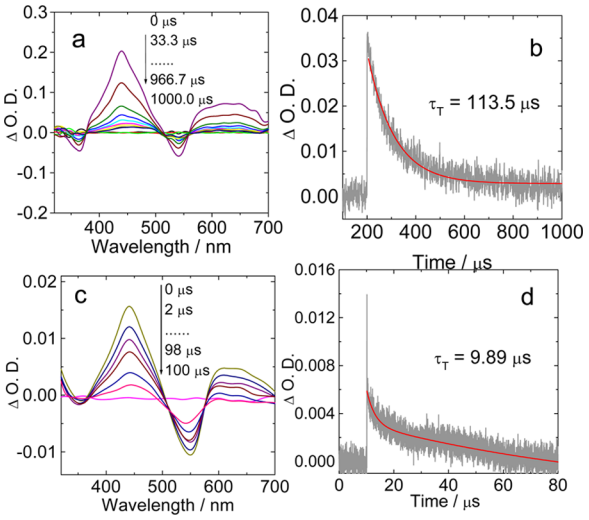

Figure 7. Switching the triplet state of **RB−NDI** by addition of TFA. Nanosecond time-resolved transient difference absorption spectra of (a) **NDI**, $c = 5.0 \times 10^{-5}$ M. Excited with 532 nm nanosecond pulsed laser. (b) Decay trace of NDI at 450 nm, $c = 1.0 \times 10^{-5}$ M. (c) **RB−NDI** in the presence of TFA (100 μL), $c = 2.0 \times 10^{-5}$ M. (d) Decay trace of **RB−NDI +TFA** at 450 nm, $c = 1.0 \times 10^{-5}$ M. Excited with 532 nm nanosecond pulsed laser. In deaerated DCM/MeOH (9/1,v/v). 20 °C. Using different concentration in the measurement of the spectra is to optimize the signal/noise ratio in the spectra and to avoid triplet−triplet annihilation effect.

Therefore, the transient signal can be attributed to the *triplet* excited state of **NDI**. In the presence of TFA, similar transient absorption profile was observed for **NDI** (τ_T = 121.6 μs, in aerated solution this lifetime was reduced to 0.77 μs, Figure S26 and S27, Supporting Information).

For **RB−NDI**, no transient signal can be detected (Figure S28, Supporting Information). The missing of the NDI triplet excited state in **RB−NDI** *cannot* be assigned to the resonance energy transfer (RET) from the NDI to RB-c moiety because RB-c does not give any absorption in visible spectral region. Therefore, the most probable quenching mechanism is electron transfer from the spirolactam rhodamine to the NDI moiety. The electrochemical data and the DFT calculations support this explanation (see later discussion).

Upon addition of acid such as TFA, transformation of RB-c → RB-o form occurred, and a transient signal similar to that of **NDI** was observed (Figure 7c). Interestingly, the bleaching band at 558 nm is more significant than the ground-state bleaching band of NDI (Figure 7a), evaluated by the intensity ratio of the bleaching band at 558 nm and the excited state absorption band at 440 nm. Considering that the steady-state absorption of rhodamine unit is similar to that of NDI, the intensified bleaching band at 558 nm may be due to the simultaneous population of the triplet state of RB-o part, besides population of the triplet excited state of the NDI moiety. Thus, we propose that the triplet state of **RB−NDI** +TFA is *delocalized* on both NDI and the rhodamine moieties; i.e., there is a triplet-state *equilibrium* in **RB−NDI+TFA**.[43] This postulation was confirmed by the DFT/TDDFT calculations on the energy levels of the triplet state of the dyads, which

Table 1. Photophysical Properties of the Compounds with and without Acid

	λ_{abs}[a] (nm)	ε[b]	λ_{em}[c] (nm)	Φ_F[d] (%)	Φ_Δ[e]	τ_T[f] (μs) (N_2)	τ_L[g] (ns)
NI	343/359	1.54/1.33	391	*k*	0.19	75.2/76.6[h]	*i*
NDI	541	1.34	570	32	0.38	113.5/121.6[h]	4.65[j]
RB	315	1.27	472	*k*	*i*	*i*	*i*
RB−NI	342/356	1.44/1.24	391	*k*	*i*	*i*	*i*
RB−NDI	537	1.08	560	*k*	*i*	*i*	0.98[g]/0.73[j]
RB+TFA	557	6.01	580	86	0.017	*i*	3.77
RB−NI+TFA	557	5.86	580	82	0.11	62.2	3.66
RB−NDI+TFA	557	6.44	578	51	0.22	9.89	1.82

[a]Maximal UV−vis absorption wavelength in DCM/MeOH = 9/1 (v/v) (1.0×10^{-5} M, 20 °C). [b]Molar absorption coefficient at absorption maxima. ε: 10^4 M^{-1} cm^{-1}. [c]Maximal emission wavelength in DCM/MeOH = 9/1 (v/v) (1.0×10^{-5} M, 20 °C). [d]The fluorescence quantum yields in DCM/MeOH = 9/1 (v/v), with 2,6-diiodo-1,3,5,7-tetramethyl-8-phenyl-4,4-difluoroboradiazaindacene (Φ_F = 2.7%, in MeCN) as the standard. [e]Singlet oxygen quantum yields in DCM (20 °C) with MB (Φ = 0.57, in DCM) as the standard. [f]Measured by transient absorption in DCM/MeOH = 9/1 (v/v) (1.0×10^{-5} M, 20 °C). [g]The fluorescence lifetime, in DCM/MeOH = 9/1 (v/v) (1.0×10^{-5} M, 20 °C). [h]In the presence of TFA. [i]Not applicable. [j]Measured in toluene (1.0×10^{-5} M, 20 °C). [k]Not observed.

dx.doi.org/10.1021/jo502554y | J. Org. Chem. 2015, 80, 568−581

indicates energetically *degenerated* T_1 and T_2 states localized on the NDI and the rhodamine moiety, respectively (see later section). Lifetime of 9.89 μs was observed. No transient signal can be detected by excitation of **RB** with TFA at 532 nm, indicated that the ISC of Rhodamine alone is extremely weak. This result indicates that the triplet-state equilibrium observed in **RB−NDI+TFA** is due to the *triplet* energy transfer from the **DNI** moiety to the rhodamine part.[11,31,32] Thus, the ISC of NDI moiety is not outcompeted by the RET effect.[10]

2.4. Electrochemical Studies: Cyclic Voltammetry. The electrochemical properties of the compounds were studied with cyclic voltammetry (Figure 8 and Table 2). For **RB** compounds, two reversible oxidation potential at +0.70 V and +0.89 V were observed. No reduction potential was observed, indicating that the RB-c is an electron donor. For NDI, four reversible reduction potentials were recorded as −0.72, −1.00, −1.22, −1.50 V, respectively (Figure S29, Supporting Information). No oxidation waves were observed up to +1.2 V. Thus, **NDI** is more likely to act as electron acceptor in the dyads. Similar results were observed for **NI** (see Supporting Information, Figure S29).

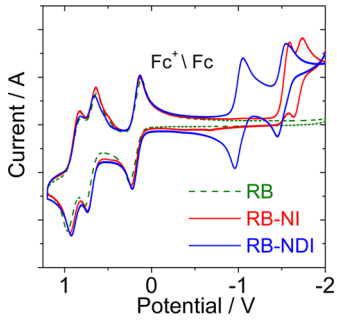

Figure 8. Cyclic voltammogram of compounds **RB**, **RB−NI**, and **RB−NDI**. Ferrocene (Fc) was used as reference. In deaerated CH_2Cl_2, 0.10 M $Bu_4N[PF_6]$ as supporting electrolyte, $Ag/AgNO_3$ reference electrode, scan rates: 100 mV/s. 20 °C.

For **RB−NDI**, two reversible oxidation potentials at +0.70 and +0.88 V were observed, which are similar to the property of RB. Two reversible reduction waves were observed for **RB−NDI** at −1.00 and −1.50 V, respectively. Similar results were found for **RB−NI**. There are two reduction waves, one is irreversible at −1.59 V and one is quasi-reversible at −1.69 V.

The photoinduced intramolecular electron transfer (PET) in **RB−NI** and **RB−NDI** was studied with the Rehm−Weller equation. We found that the free energy changes of the PET are −0.95 and −0.60 eV for **RB−NI** and **RB−NDI**, respectively, with the **RB-c** as the electron donor and the NI or NDI as electron acceptor. These negative values indicates that PET in **RB−NI** and **RB−NDI** is possible.[40,43−46] This result is in agreement with the experimental results that the NDI's fluorescence is quenched in **RB−NDI** (Figure 2a), and the triplet state of NI and NDI was also quenched in **RB−NI** and **RB−NDI** (Figure S28, Supporting Information).

2.5. DFT Calculations: Excited States. The photophysical properties of the dyads, including the controlling of the triplet states, were studied with DFT/time-dependent DFT (TDDFT) calculations.[43,47−49] First, the ground-state geometries of the dyads were optimized with the DFT method. Then the UV−vis absorption and the triplet excited state were calculated with TDDFT. The frontier molecular orbitals were analyzed; thus, the electronic transitions can be assigned.

The ground-state geometry of **RB−NDI** was optimized (Figure 9), and the UV−vis absorption of the dyad was calculated (Table 3). The frontier molecular orbitals are localized on either the RB-c part or the NDI part; thus, there is no π-conjugation between the two units. The S_1 state is a charge transfer state, thus it is expected that the singlet excited state and the triplet excited state of **RB−NDI** was quenched. Experimentally, the fluorescence of NDI was quenched and no transient signal could be detected for **RB−NDI** (see the Nanosecond Time-Resolved Transient Difference Absorption Spectroscopy section, Figure 7). An absorption band at 508 nm was predicted for which HOMO-3 → LUMO transition was involved. This absorption band can be attributed to the NDI moiety, which is in good agreement with the experimental results (537 nm, Figure 1). The triplet excited states were also calculated with the TDDFT method. HOMO-3 → LUMO transition was involved in the T_1 state; thus, the T_1 state is localized on the NDI unit.

Upon addition of TFA, thus the spirolactam → open amide transformation, the photophysical property of the **RB−NDI** changed. With TDDFT calculations on the singlet excited state (UV−vis absorption), we observed a new absorption band at 476 nm, with a large oscillator strength (f) of 0.9985. HOMO → LUMO+1 transition is involved in this absorption band (Figure 10), which is localized on the RB-o part. It is known that the B3LYP method overestimates the excitation energy for the rhodamine chromophore.[50,51]

Triplet excited-state energy levels **RB−NDI** in the presence of TFA were calculated on the basis of the ground-state

Table 2. Electrochemical Data of Compound Rhodamine B, RB, NI, NDI, RB−NI, and RB−NDI. Anodic and Cathodic Wave Potential Presented[a]

	$E_{(OX)}$ (V)	$E_{(RED)}$ (V)	ΔGcs (eV)
rhodamine B	+0.85/+0.97	−1.15/−1.37	[b]
RB	+0.70/+0.89	[b]	[b]
NI	[b]	−1.60/−1.70	[b]
NDI	[b]	−0.72/−1.00/−1.22/−1.50	[b]
RB−NI	+0.69/+0.88	−1.59/−1.69	−0.95,[c] −0.1,[d] +0.18,[e] +0.06[f]
RB−NDI	+0.70/+0.88	−1.00/−1.50	−0.60,[c] −0.06,[d] −0.40,[e] +0.09[f]

[a]Cyclic voltammetry in Ar saturated CH_2Cl_2 containing a 0.10 M Bu_4NPF_6 supporting electrolyte; counter electrode is Pt electrode; working electrode is glassy carbon electrode; $Ag/AgNO_3$ couple as the reference electrode. $c[Ag^+]$ = 0.1 M. [b]No reduction potential or no ΔGcs values. [c]The value was calculated with the singlet excited state of NI and NDI as $E_{0,0}$. [d]The value was calculated by triplet excited state of NI and NDI. [e]With the S_1 state energy level of RB-o as $E_{0,0}$ (2.13 eV). [f]With RB-o as electron donor, and the T_1 state energy level of NI and NDI as $E_{0,0}$ (see the Supporting Information).

dx.doi.org/10.1021/jo502554y | J. Org. Chem. 2015, 80, 568−581

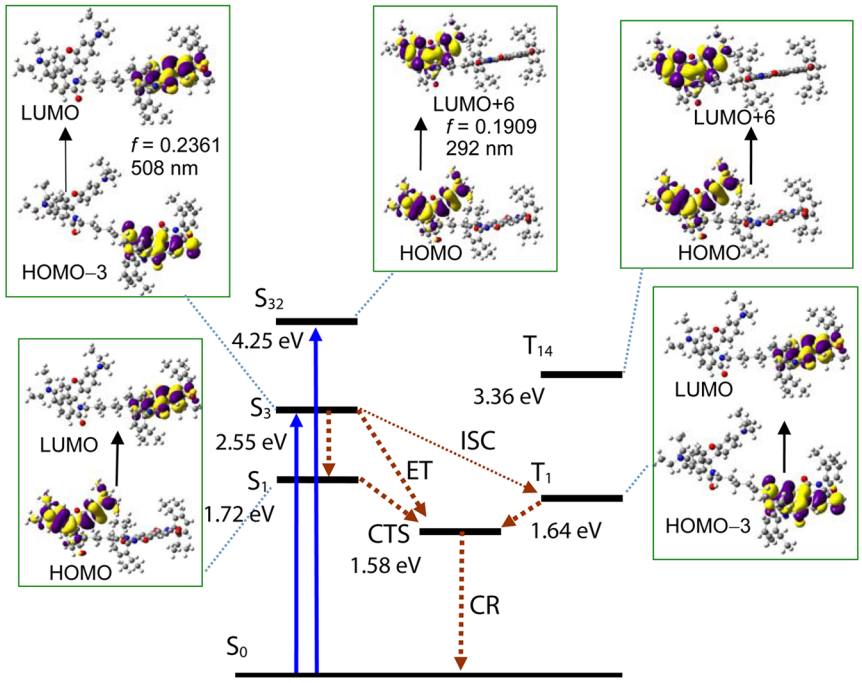

Figure 9. Selected frontier molecular orbitals involved in the excitation and triplet excited states of **RB−NDI**. The charge-transfer state (CTS) state is also presented (the energy level is derived from the electrochemical studies). CR: charge recombination, ET: electron transfer. The calculations are at the B3LYP/6-31G(d)/LANL2DZ level using Gaussian 09W.

geometry (Table 4). When the T_1 state has an energy level of 1.64 eV, HOMO−1 → LUMO transition is involved. These MOs are localized on NDI (Figure 10); thus, the T_1 state of RB(o)-NDI is localized on the NDI part. The T_2 state has a similar energy level of 1.73 eV. HOMO → LOMO+1 are involved in the T_2 state, which are localized on RB(o) part. Since these two triplet states share a similar energy level, a triplet state equilibrium is therefore expected.[43] Indeed, in the nanosecond transient difference absorption spectra of RB(o)-NDI, the bleaching band contains the contribution of both the NDI and rhodamine parts; i.e., triplet-state equilibrium was observed.

Interestingly, no low-lying charge transfer state was observed for **RB−NDI** in the presence of acid (Figure 10 and Table 4). The S_2 state is a nonemissive charge-transfer state. These findings are in agreement with the experimental results that fluorescence and triplet states were observed for **RB−NDI +TFA** (Figure 2b). Thus, the photophysical properties of **BR-NDI** in the absence and in the presence of acid are rationalized.

The DFT calculation results of **RB−NI** (see the Supporting Information, Figure S30 and S31) are similar to those of **RB−NDI**. For **RB(c)-NI**, the S_1 state is a charge-transfer state which may quench the triplet state of **NI** (no nanosecond time-resolved transient signal can be detected for **RB−NI** in the absence of TFA). In the presence of TFA, the T_1 state localized on **RB(o)** was predicted, which is in agreement with the results observed in the nanosecond time-resolved transient absorption spectra (Figure 6).

The localization of the triplet state of the dyads upon switching was studied with the spin density surface analysis (Figure 11).[14,31,32,52] For **RB(c)-NI**, the triplet state is localized on the NI moiety. For the **RB(o)-NI**, however, the triplet state is localized on the RB-o moiety. Similar results were observed for **RB−NDI**. For **RB(c)-NDI**, the triplet state is localized on the NDI moiety. This conclusion is in agreement with the TDDFT calculations on the energy level of the triplet states. For the **RB(o)-NDI**, the spin density surface is localized on NDI. This finding is in agreement with the nanosecond time-resolved transient absorption spectroscopy, in which the transient is more localized on the NDI part for **RB−NDI**.

The photophysical property of the dyad **RB−NDI** in the absence and presence of TFA can be summarized in Scheme 2. For **RB−NDI**, both the singlet and the triplet excited states of the closed lactam form of rhodamine part have *higher* energy levels than the NDI part, based on the UV−vis absorption/fluorescence spectroscopy and the DFT/TDDFT calculation data. Thus, the ISC of the NDI part is unperturbed. However, production of the T_1 state of the NDI part was inhibited by charge transfer. As a result, no long-lived triplet excited state was observed for **RB−NDI** in the absence of acid.

In the presence of TFA (Scheme 2b), the rhodamine part undertakes the spirolactam → opened amide structural transformation. The energy level of the S_1 state of the rhodamine part becomes lower than the S_1 state of NDI part (based on the UV−vis absorption spectra and fluorescence emission spectra). RET from NDI to rhodamine part competes with the ISC of NDI moiety, indicated by the quenching of the NDI's fluorescence. Electron transfer is also possible because the $^1O_2$ quantum yield of **RB-(o)-NDI** (Φ_Δ = 22%) is smaller than NDI alone (Φ_Δ = 38%). However, it is unlikely that the RET can overwhelmingly outcompete with the ISC process; otherwise, the triplet state yield of the dyad will be much lower because it is known that the rhodamine part is with very inefficient ISC.[33] The triplet state energy level of rhodamine part is slightly higher than the NDI part; thus, a triplet-state equilibrium established.[43] This conclusion is supported by the nanosecond transient difference absorption spectroscopy.

2.6. Switching of the $^1O_2$ Production. Switching of the triplet state of organic dyads will be significant for the application of these compounds in the areas such as for singlet

dx.doi.org/10.1021/jo502554y | J. Org. Chem. 2015, 80, 568−581

Table 3. Electronic Excitation Energies (eV), Corresponding Oscillator Strengths (f), Main Configurations, and CI Coefficients of the Low-Lying Electronic Excited States of the RB−NDI. Calculated by TDDFT//B3LYP/6-31G(d)/LanL2DZ Based on the Optimized Ground-State Geometries

	TDDFT//B3LYP/6-31G(d)			
electronic transition	energy[a] (eV/nm)	f[b]	composition[c]	CI[d]
$S_0 \rightarrow S_1$	1.72/719	0.0000	H-1→L	0.1168
			H→L	0.6973
$S_0 \rightarrow S_2$	1.86/666	0.0000	H-1→L	0.6973
			H→L	0.1168
$S_0 \rightarrow S_3$	2.55/508	0.2361	H-3→L	0.7040
$S_0 \rightarrow S_{15}$	3.52/353	0.2380	H-13→L	0.6659
			H-3→L+1	0.1360
			H-3→L+2	0.1036
$S_0 \rightarrow S_{23}$	3.79/327	0.1301	H-18→L	0.1519
			H-16→L	0.4603
			H-13→L	0.1567
			H-3→L+1	0.4788
$S_0 \rightarrow S_{32}$	4.25/292	0.1909	H-1→L+5	0.3197
			H-1→L+12	0.1281
			H→L+6	0.5972
$T_0 \rightarrow T_1$	1.64/758	0.0000[e]	H-3→L	0.7018
$T_0 \rightarrow T_2$	1.72/719	0.0000[e]	H-1→L	0.1168
			H→L	0.6973
$T_0 \rightarrow T_3$	1.86/666	0.0000[e]	H-1→L	0.6973
			H→L	0.1168
$T_0 \rightarrow T_{14}$	3.36/369	0.0000[e]	H-2→L+12	0.1857
			H-1→L+13	0.3243
			H→L+6	0.5347
			H→L+16	0.1281

[a]Only the selected low-lying excited states are presented. [b]Oscillator strength. [c]Only the main configurations are presented. [d]The CI coefficients are in absolute values. [e]No spin−orbital coupling effect was considered; thus, the f values are zero.

oxygen ($^1O_2$) photosensitizing.[10,15,25] The $^1O_2$ photosensitizing ability of the compounds were studied with 1,3-diphenylisobenzofuran (DPBF) as the $^1O_2$ scavenger (Scheme 3), and the production of $^1O_2$ can be monitored by following the UV−vis absorption of DPBF at 414 nm (Figure 12). **RB(c)-NI** gives weak $^1O_2$ photosensitizing ability (Figure 12a). In the presence of TFA, the $^1O_2$ photosensitizing ability increased significantly (Figure 12b).

Similar results were observed for **RB(c)-NDI**. The $^1O_2$ production ability is weak in the absence of TFA. In the presence of TFA, i.e., for the **RB(o)-NDI**, the $^1O_2$ producing ability is much stronger, indicated by the sharp decrease of the absorption of DPBF at 414 nm.

First the switching effect of protonation on the $^1O_2$ photosensitizing ability of **RB−NI** was studied. In the absence of TFA, the $^1O_2$ photosensitizing of **RB−NI** is weak. In the presence of TFA, the $^1O_2$ photosensitizing of **RB−NI** is much stronger (Figure 13). NI alone gives a strong $^1O_2$ photosensitizing effect. The reduced $^1O_2$ photosensitizing of **RB−NI +TFA** as compared with **NI** may be due to the photoinduced electron transfer, as well as the RET effect competing with the ISC of NI moiety. The $^1O_2$ photosensitizing ability of RB-o alone was also measured. Weak $^1O_2$ photosensitizing ability was found, indicating that RB-o gives very weak ISC.[33]

For **RB−NDI**, similar switching results were observed. Furthermore, the $^1O_2$ photosensitizing of **NDI** is not affected by TFA. Thus, the switching of $^1O_2$ producing ability of **RB−NDI** is attributed to the acid induced cyclic lactam → open amide structure transformation of the rhodamine moiety in **RB−NDI**. Such a acid-switched $^1O_2$ producing ability is interesting, since pH-activatable selective PDT reagents can be developed with these triplet photosensitizers.[25] Currently we are working along this line.

2.7. Intracellular Luminescent Bioimaging and Photodynamic Studies. The dyads **RB−NI** and **RB−NDI** show acid-activatable fluorescence and production of triplet excited states, thus the intracellular luminescence bioimaging and the photodynamic therapy (PDT) effect were studied, exemplified with **RB−NDI** (Figures 14−16).

RB−NDI was incubated with HeLa cells for 24 h at 37 °C. Since the fluorescence of **RB−NDI** can be activated by acid, a commercial lysosome tracker LysoTrackerGreen DND-26 (LTG) was added. Then the cells were imaged with confocal microscopy (Figure 14). In channel 1, the **RB−NDI** gives strong red emission (Figure 14a). In channel 2, the lysosome tracker gives green emission. The merged image (Figure 14c) indicates that the two channel images overlapped very well with each other, confirming that **RB−NDI** can specifically localize in the lysosomes of living cells. The changes in the intensity profile of linear regions of interest (ROIs) (**RB−NDI** and LysoTrackerGreen DND-26) show good synchronization (Figure 14e). From the intensity correlation plots (Figure 14f), a high Pearson's coefficient and overlap coefficient of 0.869 and 0.947 were obtained, respectively. The above colocalization investigation confirmed that **RB−NDI** can be activated in lysosomes specifically.

Production of $^1O_2$ in living cells with **RB−NDI** was proven by an $^1O_2$ probe, DCFH-DA (Figure 15). After incubation of the cells with **RB−NDI** and DCFH-DA, no green fluorescence were observed if no preirradiation with green LED (515−525 nm) was performed (Figure 15a). If green LED irradiation was applied for the cells after coincubation of the cells with **RB−NDI** and DCFH-DA, green fluorescence was observed (Figure 15d), indicating that $^1O_2$ was produced intracellularly.

The PDT effect of **RB−NDI** upon irradiation was studied by the Trypan Blue staining (Figure 16). With control experiments, we show that upon irradiation **RB−NDI** is effective to induce cell death, whereas the cytotoxicity of **RB−NDI** is negligible under the same conditions.

2.8. Conclusions. In conclusion, switching of the triplet excited state of rhodamine−bromonaphthaleneimide (**RB−NI**) and rhodamine−bromonaphthalenediimide (**RB−NDI**) dyads was achieved. The key to the molecular design strategy is to employ the reversible spirolactam form ↔ opened amide structure transformation of the rhodamine moiety, with which the S_1 and T_1 state energy levels of RB unit change substantially. The photophysical processes of the dyads were studied with steady-state and nanosecond time-resolved transient absorption and emission spectroscopies. The bromo-NI or the bromo-NDI units in the dyads are the triplet state producing units (intramolecular spin converter), whereas the lactam form of rhodamine moiety shows no visible light absorption and a high triplet-state energy level, but the opened amide form of rhodamine moiety shows strong absorption at 557 nm and a decreased triplet state energy level. Thus, the acid-activated fluorescence resonance energy transfer (FRET) competes with the intersystem crossing (ISC) of the NI or the

dx.doi.org/10.1021/jo502554y | J. Org. Chem. 2015, 80, 568−581

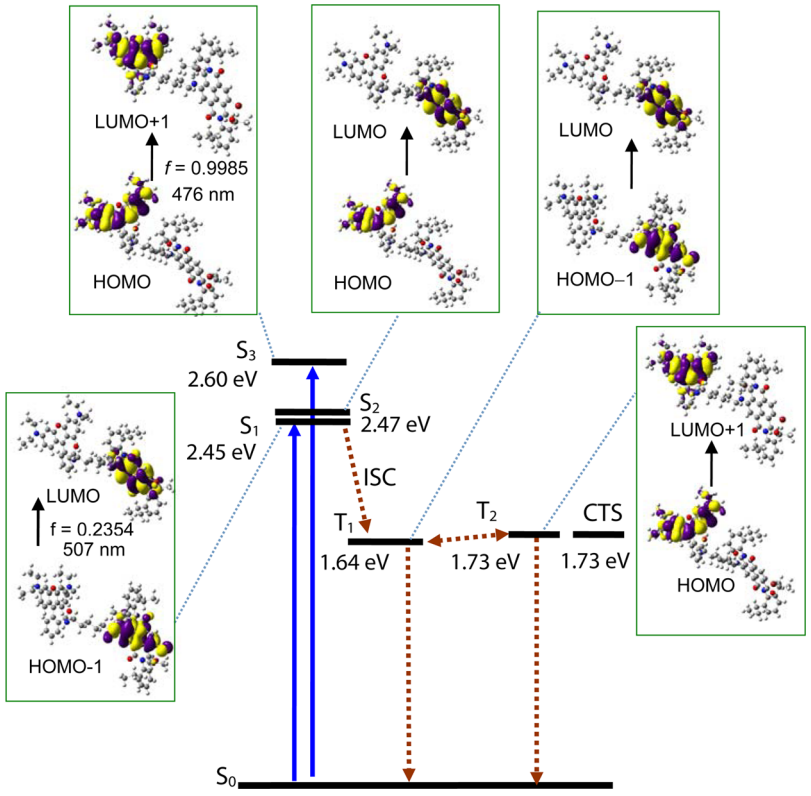

Figure 10. Selected frontier molecular orbitals involved in the excitation and triplet excited states of **RB−NDI+TFA**. The calculations are at the B3LYP/6-31G(d)/LANL2DZ level using Gaussian 09W.

Table 4. Electronic Excitation Energies (eV), Corresponding Oscillator Strengths (*f*), Main Configurations, and CI Coefficients of the Low-Lying Electronic Excited States of the Compound RB−NDI+TFA. Calculated by TDDFT//B3LYP/6-31G(d)/LanL2DZ Based on the Optimized Ground-State Geometries

	TDDFT//B3LYP/6-31G(d)			
electronic transition	energy[a] (eV/nm)	*f*[b]	composition[c]	CI[d]
$S_0 \rightarrow S_1$	2.45/507	0.2354	H-1→L	0.7040
$S_0 \rightarrow S_2$	2.47/502	0.0000	H→L	0.7071
$S_0 \rightarrow S_3$	2.60/476	0.9985	H→L+1	0.7047
$S_0 \rightarrow S_{15}$	3.51/353	0.2493	H-14→L	0.1017
			H-8→L	0.6641
			H-1→L+2	0.1304
			H-1→L+4	0.1026
$T_0 \rightarrow T_1$	1.64/754	0.0000[e]	H-1→L	0.7017
$T_0 \rightarrow T_2$	1.73/715	0.0000[e]	H→L+1	0.7056

[a]Only the selected low-lying excited states are presented. [b]Oscillator strength. [c]Only the main configurations are presented. [d]The CI coefficients are in absolute values. [e]No spin−orbital coupling effect was considered; thus, the *f* values are zero.

NDI moiety as a result the production of the triplet state was switched by adding acid/base. Interestingly, a mechanism of electron transfer dictates the production of the triplet state. In the absence of acid, no production of triplet excited state was observed for both **RB−NI** and **RB−NDI**, due to intramolecular electron transfer. With addition of acid such as trifluoroacetic acid (TFA), triplet excited states were observed for both **RB−NI** and **RB−NDI**. The singlet oxygen quantum yield (Φ_Δ) was switched from negligible to 22%, and the triplet-state lifetime

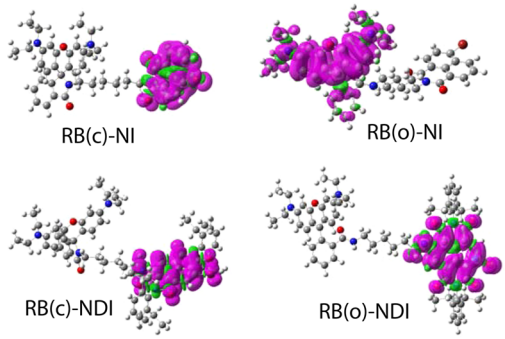

Figure 11. Isosurfaces of the spin density of **RB(c)−NI**, **RB(o)−NI**, **RB(c)−NDI**, and **RB(o)−NDI** at the optimized triplet-state geometry (isovalue: ± 0.0004). Calculated at B3LYP/6-31G(d)/LANL2DZ level with Gaussian 09W.

(τ_T) was switched from <10 ns to 62.2 μs. With nanosecond time-resolved transient absorption spectroscopy, we found the triplet excited state is localized on the rhodamine moiety for **RB−NI+TFA**. For **RB−NDI+TFA**, the triplet excited state is *delocalized* on both the rhodamine and the NDI moiety; i.e., there is triplet-state equilibrium in **RB−NDI**. Electrochemical study with cyclic voltammetry indicated that intramolecular electron transfer is thermodynamically allowed for **RB−NDI** and **RB−NI**, which is responsible for the quenching of the fluorescence as well as the triplet state (in the absence of acid). The photophysical properties of these triplet excited state are rationalized by DFT/TDDFT calculations. Intracellular lysosome-specific staining and photodynamic therapy were also studied. These investigations shed light on the rarely studied triplet excited-state switching in organic chromophores, and the

dx.doi.org/10.1021/jo502554y | J. Org. Chem. 2015, 80, 568−581

Scheme 2. Simplified Jablonski Diagram Illustrating the Photophysical Processes Involved in (a) RB−NDI and (b) RB−NDI in the Presence of TFA[a]

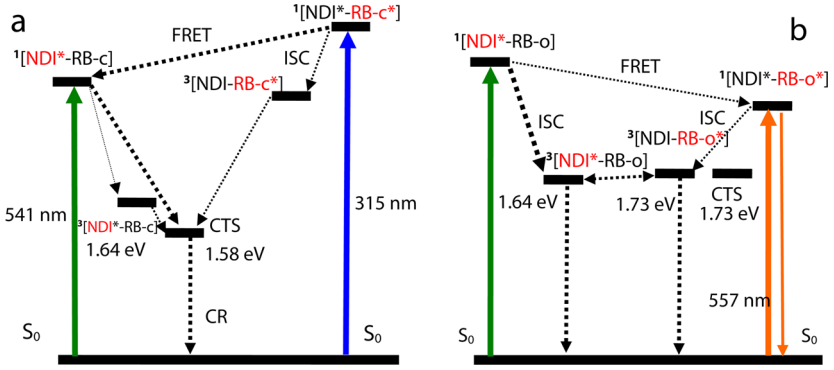

[a]Keys: [NDI-RB-c] stands for **RB−NDI** with rhodamine part in the closed lactam structure. [NDI-RB-o] stands for **RB−NDI** with rhodamine part in the opened amide structure. CTS stands for charge-transfer state. CR stands for charge recombination. The localization of the excited state in dyads is designated in red. The number of the superscript designates the spin multiplicity. Note in ^{1}[NDI-RB-o] the ISC process of the NDI part competes with the FRET process, with the rhodamine moiety as singlet energy acceptor.

Scheme 3. Mechanism for Monitoring the $^1O_2$ Production of the Dyads with DPBF as $^1O_2$ Scavenger

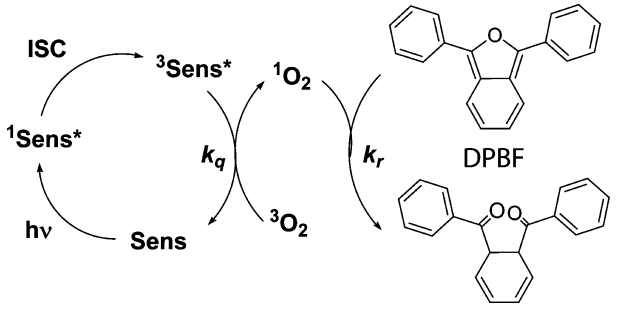

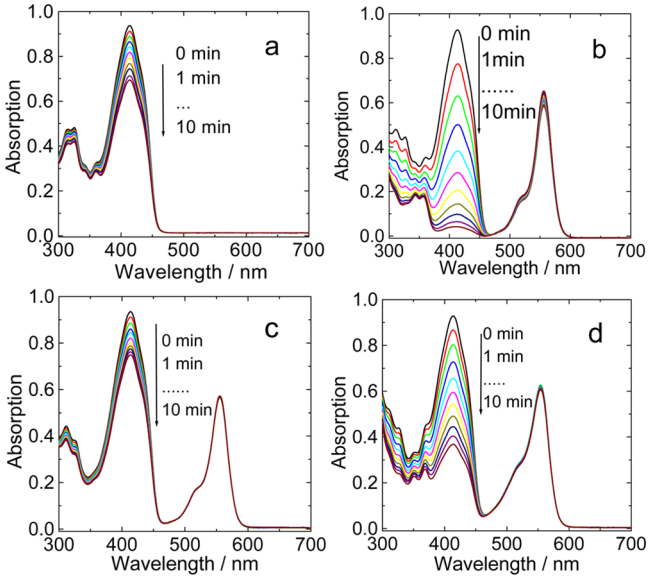

Figure 12. UV−vis absorption spectral change for the photooxidation of **DPBF** using compound (a) **RB−NI** (b) **RB−NI+TFA** as photosensitizers. With TFA (5.0 mol/L, 50 μL) added. c [DPBF] = 3.33×10^{-5} M. λ_{ex} = 350 nm. c = 1.0×10^{-5} M. 20 °C. (c) **RB+TFA** and (d) **RB−NDI+TFA** as photosensitizers. With TFA (5.0 mol/L, 50 μL) added. c [DPBF] = 3.33×10^{-5} M. λ_{ex} = 500 nm. c = 1.0×10^{-5} M in DCM:CH_3OH (9:1, v/v). 20 °C.

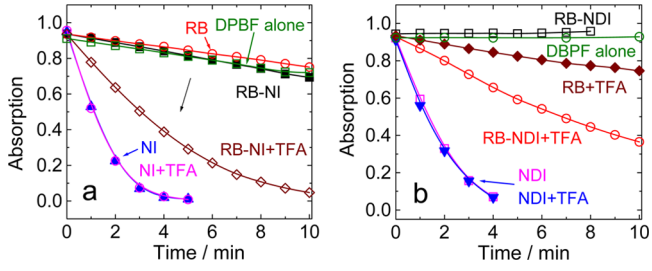

Figure 13. Demonstration of the acid-switching of the $^1O_2$ photosensitizing ability of the photosensitizers. 1,3-diphenylisobenzofuran (DPBF) was used as the $^1O_2$ scavenger, the absorption changes of DPBF at 414 nm upon photoirradiation was used to follow the $^1O_2$ production. with TFA (5 mol/L, 50 μL) added. (a) **RB−NI**. Excited at 350 nm. (b) **RB−NDI**. Excited at 500 nm. 20 °C.

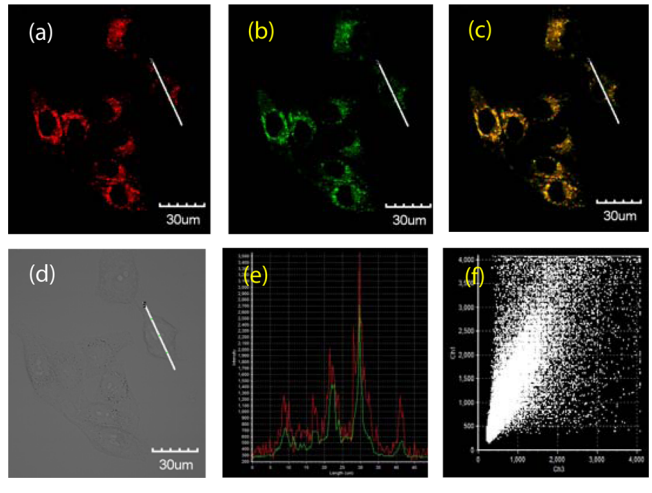

Figure 14. Confocal microscopy images of HeLa cells treated with **RB−NDI** and LysoTrackerGreen DND-26 (LTG). Cells were incubated with **RB−NDI** (15.0 μM) for 24 h at 37 °C and LTG (2.5 μM) for 2 min. The excitation wavelength was 488 nm, and images were collected at (a) 560−660 nm and (b) 490−530 nm. (c) Merged images. (d) Corresponding contrast image. (e) Intensity profile of ROIs across HeLa cells. (f) Correlation plot of LTG and **RB−NDI** intensities.

dx.doi.org/10.1021/jo502554y | J. Org. Chem. 2015, 80, 568−581

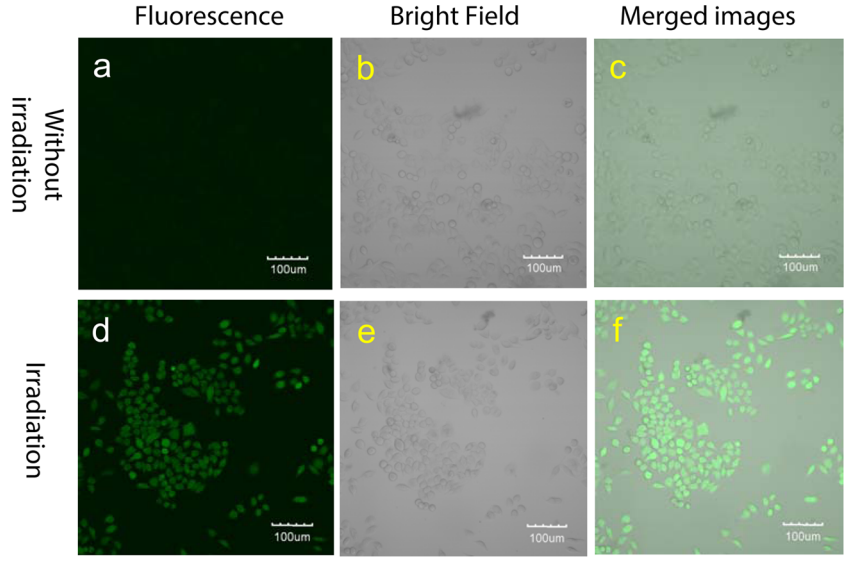

Figure 15. Confocal microscopy images of HeLa cells treated with **RB−NDI** and DCFH−DA. Cells were incubated with **RB−NDI** (15.0 μM) for 24 h at 37 °C and DCFH−DA (10 μM) for 2 min before luminescence imaging studies. The excitation wavelength was 488 nm, and images were collected at (a, d) 500−530 nm. (b, e) The corresponding contrast image. (c, f) Merged images. No light irradiation was applied for (a−c). Irradiation with 515−525 nm LED for 3 min was applied for the cells of (d−f). 37 °C.

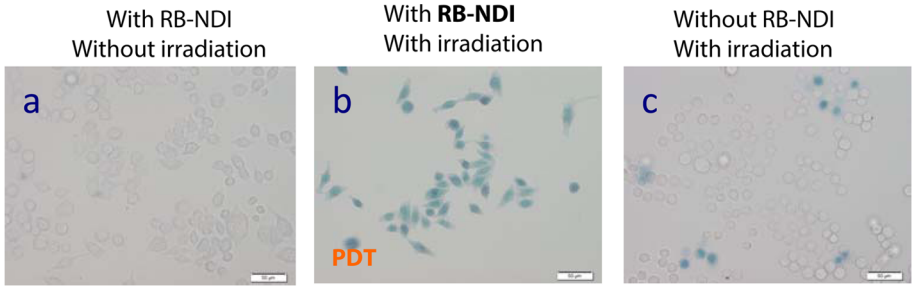

Figure 16. Photocytotoxic activity of the sensitizers with Trypan blue staining images of HeLa cells. (a) Cells were incubated with **RB−NDI** and were kept in the dark for 24 h in the same incubator before Trypan blue staining. (b) Cells were incubated with **RB−NDI** for 24 h in the dark then was illuminated with 515−525 nm LED for 2 h before Trypan blue staining. The dead cells are preferentially stained with Trypan blue because of increased cellular permeability. (c) Cells were incubated for 24 h in the absence of **RB−NDI** and then illuminated for 2 h with green LED before the Trypan blue staining. The concentration of **RB−NDI** was at 15 μM. 37 °C.

results will be useful for designing external stimuli-activatable triplet photosensitizers, which is useful for study of activatable photodynamic therapeutic reagents, molecular devices such as logic gates, as well as for the study of the photochemistry of organic molecular arrays.

3. EXPERIMENTAL SECTION

3.1. General Methods. All of the chemicals used in the synthesis are analytical pure and were used as received. Fluorescence quantum yields were measured with 2,6-diiodo-1,3,5,7-tetramethyl-8-phenyl-4,4-difluoroboradiazaindacene (2,6-diiodoBodipy) as standard (Φ_F = 0.027 in MeCN). The fluorescence lifetimes of the compounds were measured with EPL picosecond pulsed laser (473 nm, pulse width: 66.9 ps, maximum average power: 5 mW; Edinburgh Instrument Ltd., UK), which was synchronized to the FLS 920 spectrofluorometer. The fluorescence and kinetic curve (fluorescence emission) was recorded with a RF 5301PC spectrofluorometer.

3.2. Compound 1. Under Ar atmosphere, a solution of rhodamine B (500.0 mg, 1.04 mmol) and 1,6-hexanediamine (600.0 mg, 5.17 mmol) was refluxed in EtOH (10 mL) for 12 h until the solution color changed from pink to colorless. After the solution was cooled to room temperature, the solvent was evaporated under reduced pressure, CH_2Cl_2 (100 mL) and water (200 mL) were added, and the organic layer was separated. The organic layer was washed with water and dried over anhydrous Na_2SO_4. The crude product was purified with column chromatography (silica gel, CH_2Cl_2/triethylamine = 20:1, v/v) to give 490.0 mg of white solid. Yield: 88%. Mp: 36.9−38.3 °C. ^{1}H NMR (400 MHz, $CDCl_3$): δ 7.89 (t, 1H, J = 8.0 Hz), 7.43−7.41 (m, 2H), 7.08−7.06 (m, 1H), 6.43−6.38 (m, 4H), 6.28−6.25 (m, 2H), 3.36 (q, 8H, J = 20.0 Hz), 3.11 (t, 2H, J = 12.0 Hz), 2.71 (t, 2H, J = 16.0 Hz), 1.42 (t, 2H, J = 12.0 Hz), 1.18−1.11 (m, 20H). MALDI-HRMS (TOF): calcd ($[C_{34}H_{44}N_4O_2 + H]^+$) m/z = 541.3543, found m/z = 541.3517.

3.3. Compound RB. The synthesis of **RB** is similar to that of **1**. Under Ar atmosphere, the mixture of rhodamine B (200.0 mg, 0.42 mmol), *n*-butylamine (91.0 mg, 1.25 mmol), and EtOH (5 mL) was refluxed for 8 h until the solution changed from pink to colorless. After evaporation of the solvent under reduced pressure, the residue was repatriated in water-dichloromethane (DCM). The organic layer was separated and dried over Na_2SO_4. The crude product was purified with column chromatography (silica gel, CH_2Cl_2/ethyl acetate =

dx.doi.org/10.1021/jo502554y | J. Org. Chem. 2015, 80, 568−581

10:1, v/v) to give 180.0 mg of white solid. Yield: 87%. Mp: 165.9−166.6 °C. ^{1}H NMR (400 MHz, $CDCl_3$): δ 7.90 (t, 1H, J = 8.0 Hz), 7.43 (t, 2H, J = 8.0 Hz), 7.08 (t, 1H, J = 8.0 Hz), 6.45−6.26 (m, 6H), 3.36 (q, 8H, J = 20.0 Hz), 3.12 (t, 2H, J = 12.0 Hz), 1.18 (t, 12H, J = 12.0 Hz), 1.11−1.09 (m, 4H), 0.69 (t, 3H, J = 12.0 Hz). ^{13}C NMR (100 MHz, $CDCl_3$): δ 168.1, 153.7, 154.3, 148.8, 132.2, 131.8, 131.7, 129.1, 128.0, 123.8, 122.8, 108.1, 106.2, 97.8, 65.0, 44.5, 40.3, 30.5, 20.5, 13.8, 12.7. MALDI-HRMS (TOF): calcd ($[C_{32}H_{39}N_3O_2 + H]^+$), m/z = 498.3121, found m/z = 498.3147.

3.4. Compound RB−NI. Under Ar atmosphere, a mixture of **1** (120.0 mg, 0.25 mmol) and **2** (68.0 mg, 0.25 mmol) was refluxed in EtOH (10 mL) for 8 h. After evaporation of the solvents under reduced pressure, the crude product was purified with column chromatography (silica gel, CH_2Cl_2/ethyl acetate = 10:1, v/v) to give 168.0 mg of white-yellow solid. Yield: 83%. Mp: 127.6−129.5 °C. ^{1}H NMR (400 MHz, $CDCl_3$): δ 8.64 (d, 1H, J = 8.0 Hz), 8.57 (d, 1H, J = 8.0 Hz), 8.40 (d, 1H, J = 8.0 Hz), 8.04 (d, 1H, J = 8.0 Hz), 7.88−7.82 (m, 2H), 7.42 (s, 2H), 7.07 (t, 1H, J = 8.0 Hz), 6.44 (d, 2H, J = 8.0 Hz), 6.37 (s, 2H), 6.27 (d, 2H, J = 8.0 Hz), 4.06 (t, 2H, J = 16.0 Hz), 3.15 (q, 8H, J = 24.0 Hz), 3.09 (s, 2H), 1.59−1.51 (m, 4H), 1.25 (s, 4H), 1.16 (t, 12H, J = 12.0 Hz). ^{13}C NMR (100 MHz, $CDCl_3$): δ 168.1, 163.6, 153.7, 153.4, 148.8, 132.1, 130.7, 129.1, 128.2, 128.0, 123.8, 123.3, 122.8, 122.4, 108.1, 106.1, 97.8, 65.0, 44.5, 40.6, 29.9, 28.3, 28.1, 27.2, 26.9,12.8. MALDI-HRMS (TOF): calcd ($[C_{46}H_{47}N_4O_4Br + H]^+$) m/z = 799.2859, found m/z = 799.2898.

3.5. Compound RB−NDI. Under Ar atmosphere, a mixture of **1** (40.0 mg, 0.074 mmol) and **3** (55.0 mg, 0.074 mmol) was refluxed in 2-methoxyethanol (5 mL) for 8 h. After being cooled to room temperature, the solvent was evaporated under reduced pressure. Then the crude product was purified with column chromatography (silica gel, CH_2Cl_2/ethyl acetate = 100:1, v/v) to give 30.0 mg of red solid. Yield: 33%. Mp: 150.8−152.7 °C. ^{1}H NMR (400 MHz, $CDCl_3$): δ 9.97 (s, 1H), 8.99 (s, 1H), 8.31 (s, 1H), 7.88 (d, 1H, J = 4.0 Hz), 7.52−7.47 (m, 2H), 7.43 (s, 2H), 7.36 (t, 4H, J = 12.0 Hz), 7.06 (d, 1H, J = 8.0 Hz), 6.42−6.26 (m, 6H), 3.48 (t, 2H, J = 16.0 Hz), 3.34−3.29 (m, 8H), 3.10−3.06 (m, 2H), 2.70−2.62 (m, 4H), 1.17−1.09 (m, 44H). ^{13}C NMR (100 MHz, CD_2Cl_2): δ 168.0, 166.5, 162.5, 162.0, 153.6, 152.6, 149.1, 146.3, 146.2, 138.8, 132.4, 131.9, 131.1, 129.9, 129.2, 128.3, 128.1, 124.5, 124.2, 123.8, 122.7, 121.7, 120.6, 108.3, 106.3, 100.1, 97.9, 64.9, 44.7, 43.7, 40.3, 30.0, 29.6, 29.5, 29.2, 28.4, 26.9, 24.0, 12.7. MALDI-HRMS (TOF): calcd ($[C_{72}H_{79}N_6O_6Br + H]^+$), m/z = 1203.5323, found m/z = 1203.5293.

3.6. Compound NDI. The mixture of compound **3** (150.0 mg, 0.2 mmol), 2-ethylhexylamine (26.0 mg, 0.2 mmol), and 2-methoxyethanol (5 mL) was stirred at 120 °C for 8 h. After removal of 2-methoxyethanol under reduced pressure, the residue was purified with column chromatography (silica gel, dichloromethane/petroleum ether = 1:1, v/v) to give 84.0 mg of a red solid. Yield: 54.0%. Mp: 88.2−90.2 °C. ^{1}H NMR (400 MHz, $CDCl_3$): δ 10.16 (s, 1H), 8.99 (s, 1H), 8.40 (s, 1H), 7.54 (q, 2H, J = 24.0 Hz), 7.38 (t, 4H, J = 20.0 Hz), 3.52 (t, 2H, J = 12.0 Hz), 2.73−2.64 (m, 4H), 1.26−1.14 (m, 33H), 0.92−0.85 (m, 6H) ^{13}C NMR (100 MHz, $CDCl_3$): δ 166.4, 162.0, 161.6, 160.9, 152.6, 145.6, 145.5, 139.6, 138.9, 130.4, 130.2, 139.9, 129.1, 128.0, 124.4, 124.3, 123.9, 122.5, 121.3, 120.8, 100.0, 46.6, 39.4, 37.9, 33.8, 31.2, 29.4, 28.8, 24.5, 24.0, 13.0, 14.0, 11.0. MALDI-HRMS (TOF): calcd ($[C_{46}H_{54}N_3O_4Br]^-$) m/z = 791.3298, found m/z = 791.3306.

3.7. Nanosecond Time-Resolved Transient Difference Absorption Spectra. The nanosecond time-resolved transient difference absorption spectra were measured on LP920 laser flash photolysis spectrometer (Edinburgh Instruments, UK) and recorded on a Tektronix TDS 3012B oscilloscope. The lifetime values (by monitoring the decay trace of the transients) were obtained with the LP900 software. All samples in flash photolysis experiments were deaerated with N_2 for ca. 15 min before measurement, and the gas flow was maintained during the measurement. For the samples with TFA added, the solution was allowed to stand for 1 h before measurement.

3.8. Cyclic Voltammetry. Cyclic voltammetry was performed using a CHI610D electrochemical workstation (Shanghai, China). Cyclic voltammograms were recorded at scan rates of 0.1 V/s. The electrolytic cell used was a three-electrode cell. Electrochemical measurements were performed at rt using 0.1 M tetrabutylammonium hexafluorophosphate ($Bu_4N[PF_6]$) as supporting electrolyte. The solution was purged with N_2 before measurement. The working electrode was a glassy carbon electrode, and the counter electrode was a platinum electrode. A nonaqueous $Ag/AgNO_3$ (0.1 M in acetonitrile) reference electrode was contained in a separate compartment connected to the solution via semipermeable membrane. DCM was used as the solvent. Ferrocene was added as the internal references.

3.9. DFT Calculations. The density functional theory (DFT) calculations were used for optimization of the ground-state geometries of both singlet states and triplet states. The energy levels of the triplet state were calculated with time-dependent DFT (TD-DFT), based on the optimized singlet ground-state geometries (S_0 state). The 6-31G(d) atomic basis set was used to determine geometrical and vibrational parameters. All calculations were performed with the Gaussian 09 program.[54]

3.10. Colocalization Experiments. HeLa (human cervical cancer) cell lines were obtained from ATCC cultured in Dulbecco's modified Eagle's medium (Invitrogen, Auckland, New Zealand) containing 10% fetal bovine serum (Hyclone, Beijing, China) and penicillin−streptomycin (100 U/mL penicillin and 0.1 mg/mL streptomycin). Cells were incubated at 37 °C in a humidified incubator (SANYO, MCO-15AC, Japan) with 5% CO_2. Then Hela cells were incubated with **RB−NI** and **RB−NDI** for another 24 h, and then prior to imaging, the medium was removed and the cells were washed three times with phosphate buffered saline (PBS, Gibco, pH = 7.4). Florescent images were acquired on a FV1000 confocal laser-scanning microscope (Olympus) with an objective lens (×100). Other information is available in the figure captions. The excitation wavelength was 488 nm, respectively. First, the image was collected at 560−660 nm for RB fluorescence, and then LysoTrackerGreen DND-26 (LTG, 2.5 μM) was added and stirred at 2 min (do not move the Confocal Petri dish), the image was collected at 490−530 nm for LTG. All images were analyzed by OLYMPUS FV1000 software.

3.11. Intracellular Singlet Oxygen Detection. After the Hela cells were incubated with **RB−NI** (**RB−NDI**) and washed three times with phosphate-buffered saline (PBS, Gibco, pH = 7.4), they were further incubated with 10 μM DCFH-DA for 2 min and irradiated with a 515−525 nm LED for 3 min at 37 °C to perform the fluorescence detection of DCF with FV1000 confocal microscopy (Olympus) with an objective lens (×20), respectively.

dx.doi.org/10.1021/jo502554y | J. Org. Chem. 2015, 80, 568−581

3.12. Intracellular Photodynamic Studies. Hela cell culture was same as that used for the colocalization experiments. Prior to imaging, the medium was removed. Cell imaging was carried out after the cells were washed with phosphate-buffered saline (PBS, Gibco, pH = 7.4) three times, and 1 mL of PBS was added to the laser scanning confocal Petri dish (nest, Glass bottom diameter: 20 mm). The cells were irradiated with a 515−525 nm LED for 120 min (**RB−NI**, **RB−NDI**) at 37 °C. Afterward, the cells were stained with Trypan blue (100 μL 0.4% Trypan blue was added); 3 min later, the cell images were acquired on IX81 confocal laser-scanning microscope (Olympus) with an objective lens (×40). Other information is available in the figure captions.

■ ASSOCIATED CONTENT

Supporting Information

Experimental procedures, molecular structure characterization, additional spectra. This material is available free of charge via the Internet at http://pubs.acs.org.

■ AUTHOR INFORMATION

Corresponding Authors

*E-mail: zhaojzh@dlut.edu.cn.
*E-mail: wuhj@dlut.edu.cn.
*E-mail: klhan@dicp.ac.cn.

Notes

The authors declare no competing financial interest.

■ ACKNOWLEDGMENTS

We thank the NSFC (21073028, 21273028, 21473020, and 21421005), the Royal Society (UK), and NSFC (China−UK Cost-Share Science Networks, 21011130154), Ministry of Education (SRFDP-20120041130005), the Fundamental Research Funds for the Central Universities (DUT14ZD226), State Key Laboratory of Fine Chemicals (KF1203), Program for Changjiang Scholars and Innovative Research Team in University [IRT_132206], and Dalian University of Technology for financial support (DUT2013TB07).

■ REFERENCES

(1) Yogo, T.; Urano, Y.; Ishitsuka, Y.; Maniwa, F.; Nagano, T. *J. Am. Chem. Soc.* **2005**, *127*, 12162−12163.
(2) Schmitt, F.; Freudenreich, J.; Barry, N. P. E.; Juillerat-Jeanneret, L.; Süss-Fink, G.; Therrien, B. *J. Am. Chem. Soc.* **2012**, *134*, 754−757.
(3) (a) Gorman, A.; Killoran, J.; O'Shea, C.; Kenna, T.; Gallagher, W. M.; O'Shea, D. F. *J. Am. Chem. Soc.* **2004**, *126*, 10619−10631. (b) Tian, J.; Ding, L.; Xu, H.-J.; Shen, Z.; Ju, H.; Jia, L.; Bao, L.; Yu, J.-S. *J. Am. Chem. Soc.* **2013**, *135*, 18850−18858.
(4) Kamkaew, A.; Lim, S. H.; Lee, H. B.; Kiew, L. V.; Chung, L. Y.; Burgess, K. *Chem. Soc. Rev.* **2013**, *42*, 77−88.
(5) (a) Awuah, S. G.; You, Y. *RSC Adv.* **2012**, *2*, 11169−11183. (b) Yang, Y.; Guo, Q.; Chen, H.; Zhou, Z.; Guo, Z.; Shen, Z. *Chem. Commun.* **2013**, *49*, 3940−3942.
(6) Cakmak, Y.; Kolemen, S.; Duman, S.; Dede, Y.; Kilic, B.; Kostereli, Z.; Yildirim, L. T.; Dogan, A. L.; Guc, D.; Akkaya, E. U. *Angew. Chem., Int. Ed.* **2011**, *50*, 11937−11941.
(7) Ozlem, S.; Akkaya, E. U. *J. Am. Chem. Soc.* **2009**, *131*, 48−49.
(8) Zhao, J.; Wu, W.; Sun, J.; Guo, S. *Chem. Soc. Rev.* **2013**, *42*, 5323−5351.
(9) (a) Lalevée, J.; Peter, M.; Dumur, F.; Gigmes, D.; Blanchard, N.; Tehfe, M. A.; Morlet-Savary, F.; Fouassier, J. P. *Chem.—Eur. J.* **2011**, *17*, 15027−15031. (b) Meng, Q.-Y.; Zhong, J.-J.; Liu, Q.; Gao, X.-W.; Zhang, H.-H.; Lei, T.; Li, Z.-J.; Feng, K.; Chen, B.; Tung, C.-H.; Wu, Li-Z. *J. Am. Chem. Soc.* **2013**, *135*, 19052−19055.
(10) Erbas-Cakmak, S.; AltanáBozdemir, O.; Cakmaka, Y.; Akkaya, E. U. *Chem. Sci.* **2013**, *4*, 858−862.
(11) Whited, M. T.; Djurovich, P. I.; Roberts, S. T.; Durrell, A. C.; Schlenker, C. W.; Bradforth, S. E.; Thompson, M. E. *J. Am. Chem. Soc.* **2011**, *133*, 88−96.
(12) (a) Lazarides, T.; McCormick, T. M.; Wilson, K. C.; Lee, S.; McCamant, D. W.; Eisenberg, R. *J. Am. Chem. Soc.* **2011**, *133*, 350−364. (b) Colombo, A.; Dragonetti, C.; Marinotto, D.; Righetto, S.; Roberto, D.; Tavazzi, S.; Escadeillas, M.; Guerchais, V.; Le Bozec, H.; Boucekkine, A.; Latouche, C. *Organometallics* **2013**, *32*, 3890−3894.
(13) Wu, W.; Zhao, J.; Sun, J.; Guo, S. *J. Org. Chem.* **2012**, *77*, 5305−5312.
(14) Guo, S.; Ma, L.; Zhao, J.; Küçüköz, B.; Karatay, A.; Hayvali, M.; Yaglioglu, H. G.; Elmali, A. *Chem. Sci.* **2014**, *5*, 489−500.
(15) Erbas-Cakmak, S.; Akkaya, E. U. *Angew. Chem., Int. Ed.* **2013**, *52*, 11364−11368.
(16) (a) De Silva, A. P.; Gunaratne, H. Q. N.; Gunnlaugsson, T.; Huxley, A. J. M.; McCoy, C. P.; Rademacher, J. T.; Rice, T. E. *Chem. Rev.* **1997**, *97*, 1515−1566. (b) Uchiyama, S.; McClean, G. D.; Iwai, K.; de Silva, A. P. *J. Am. Chem. Soc.* **2005**, *127*, 8920−8921. (c) Magri, D. C.; Brown, G. J.; McClean, G. D.; de Silva, A. P. *J. Am. Chem. Soc.* **2006**, *128*, 4950−4951. (d) Wang, L.; Qin, W.; Tang, X.; Dou, W.; Liu, W. *J. Phys. Chem. A* **2011**, *115*, 1609−1616. (e) Guo, Y.; Dou, W.; Zhou, X.; Liu, W.; Qin, W.; Zang, Z.; Zhang, H.; Wang, D. *Inorg. Chem.* **2009**, *48*, 3581−3590.
(17) Fan, J.; Hu, M.; Zhan, P.; Peng, X. *Chem. Soc. Rev.* **2013**, *42*, 29−43.
(18) Chen, X.; Zhou, Y.; Peng, X.; Yoon, J. *Chem. Soc. Rev.* **2010**, *39*, 2120−2135.
(19) Altan Bozdemir, O.; Erbas-Cakmak, S.; Ekiz, O. O.; Dana, A.; Akkaya, E. U. *Angew. Chem., Int. Ed.* **2011**, *50*, 10907−10912.
(20) (a) Srikun, D.; Miller, E. W.; Domaille, D. W.; Chang, C. J. *J. Am. Chem. Soc.* **2008**, *130*, 4596−4597. (b) Wu, Y.; Xie, Y.; Zhang, Q.; Tian, H.; Zhu, W.; Li, A. D. Q. *Angew. Chem., Int. Ed.* **2014**, *53*, 2090−2094. (c) Chen, Y.; Wang, H.; Wan, L.; Bian, Y.; Jiang, J. *J. Org. Chem.* **2011**, *76*, 3774−3781. (d) Cheng, T.; Xu, Y.; Zhang, S.; Zhu, W.; Qian, X.; Duan, L. *J. Am. Chem. Soc.* **2008**, *130*, 16160−16161. (e) Kim, S. K.; Lee, D. H.; Hong, J.-I.; Yoon, J. *Acc. Chem. Res.* **2009**, *42*, 23−31. (f) Huang, Y.-J.; Ouyang, W.-J.; Wu, X.; Li, Z.; Fossey, J. S.; James, T. D.; Jiang, Y.-B. *J. Am. Chem. Soc.* **2013**, *135*, 1700−1703. (g) Kim, K.; Choi, S. H.; Jeon, J.; Lee, H.; Huh, J. O.; Yoo, J.; Kim, J. T.; Lee, C.-H.; Lee, Y. S.; Churchill, D. G. *Inorg. Chem.* **2011**, *50*, 5351−5360. (h) Murale, D. P.; Kim, H.; Choi, W. S.; Churchill, D. G. *Org. Lett.* **2013**, *15*, 3630−3633. (i) Manjare, S. T.; Kim, S.; Heo, W. D.; Churchill, D. G. *Org. Lett.* **2014**, *16*, 410−412.
(21) Ziessel, R.; Harriman, A. *Chem. Commun.* **2011**, *47*, 611−631.
(22) (a) Feng, K.; Yu, M.-L.; Wang, S.-M.; Wang, G.-X.; Tung, C.-H.; Wu, L.-Z. *ChemPhysChem* **2013**, *14*, 198−203. (b) Lamola, A. A.; Leermakers, P. A.; Byers, G. W.; Hammond, G. S. *J. Am. Chem. Soc.* **1965**, *87*, 2322−2332. (c) Sigman, M. E.; Closs, G. L. *J. Phys. Chem.* **1991**, *95*, 5012−5017.
(23) (a) Jukes, R. T. F.; Adamo, V.; Hartl, F.; Belser, P.; De Cola, L. *Inorg. Chem.* **2004**, *43*, 2779−2792. (b) Ko, C.-C.; Kwok, W.-M.; Yam, V. W.-W.; Phillips, D. L. *Chem.—Eur. J.* **2006**, *12*, 5840−5848.
(24) (a) Tan, W.; Zhang, Q.; Zhang, J.; Tian, H. *Org. Lett.* **2009**, *11*, 161−164. (b) Boixel, J.; Guerchais, V.; Le Bozec, H.; Jacquemin, D.; Amar, A.; Boucekkine, A.; Colombo, A.; Dragonetti, C.; Marinotto, D.; Roberto, D.; Righetto, S.; De Angelis, R. *J. Am. Chem. Soc.* **2014**, *136*, 5367−5375. (c) Ordronneau, L.; Nitadori, H.; Ledoux, I.; Singh, A.; Williams, J. A. G.; Akita, M.; Guerchais, V.; Le Bozec, H. *Inorg. Chem.* **2012**, *51*, 5627−5636.
(25) McDonnell, S. O.; Hall, M. J.; Allen, L. T.; Byrne, A.; Gallagher, W. M.; O'Shea, D. F. *J. Am. Chem. Soc.* **2005**, *127*, 16360−16361.
(26) (a) Othman, A. B.; Lee, J. W.; Wu, J.-S.; Kim, J. S.; Abidi, R.; Thuéry, P.; Strub, J. M.; Van Dorsselaer, A.; Vicens, J. *J. Org. Chem.* **2007**, *72*, 7634−7640. (b) Wang, C.; Wong, K. M.-C. *Inorg. Chem.* **2013**, *52*, 13432−13441.
(27) Yuan, L.; Lin, W.; Xie, Y.; Chen, B.; Zhu, S. *J. Am. Chem. Soc.* **2011**, *134*, 1305−1315.

(28) Zhang, X.; Xiao, Y.; Qian, X. *Angew. Chem., Int. Ed.* **2008**, *47*, 8025−8029.
(29) Zhang, X.; Xiao, Y.; Qian, X. *Org. Lett.* **2008**, *10*, 29−32.
(30) Yang, P.; Wu, W.; Zhao, J.; Huang, D.; Yi, X. *J. Mater. Chem.* **2012**, *22*, 20273−20283.
(31) Huang, L.; Yu, X.; Wu, W.; Zhao, J. *Org. Lett.* **2012**, *14*, 2594−2597.
(32) Huang, L.; Cui, X.; Therrien, B.; Zhao, J. *Chem.—Eur. J.* **2013**, *19*, 17472−17482.
(33) Targowski, P.; Zietek, B. *SPIE* **1990**, *1391*, 12−17.
(34) Guo, S.; Wu, W.; Guo, H.; Zhao, J. *J. Org. Chem.* **2012**, *77*, 3933−3943.
(35) Doria, F.; Manet, I.; Grande, V.; Monti, S.; Freccero, M. *J. Org. Chem.* **2013**, *78*, 8065−8073.
(36) Stracke, F.; Heupel, Ma.; Thiel, E. *J. Photochem. Photobiol. A: Chem.* **1999**, *126*, 51−58.
(37) Turro, N. J.; Ramamurthy, V.; Scaiano, J. C. *Principles of Molecular Photochemistry: An Introduction*; University Science Books: Sausalito, CA, 2009.
(38) Suraru, S.-L.; Würthner, F. *J. Org. Chem.* **2013**, *78*, 5227−5238.
(39) Bhosale, S. V.; Jani, C.; Lalander, C. H.; Langford, S. J. *Chem. Commun.* **2010**, *46*, 973−975.
(40) Yuan, M.; Yin, X.; Zheng, H.; Ouyang, C.; Zuo, Z.; Liu, H.; Li, Y. *Chem.—Asian. J.* **2009**, *4*, 707−713.
(41) El-Khouly, M. E.; Amin, A. N.; Zandler, M. E.; Fukuzumi, S.; D'Souza, F. *Chem.—Eur. J.* **2012**, *18*, 5239−5247.
(42) Czaplyski, W. L.; Purnell, G. E.; Roberts, C. A.; Allred, R. M.; Harbron, E. J. *Org. Biomol. Chem.* **2014**, *12*, 526−533.
(43) Zhang, C.; Zhao, J.; Wu, S.; Wang, Z.; Wu, W.; Ma, J.; Guo, S.; Huang, L. *J. Am. Chem. Soc.* **2013**, *135*, 10566−10578.
(44) Bura, T.; Nastasi, F.; Puntoriero, F.; Campagna, S.; Ziessel, R. *Chem.—Eur. J.* **2013**, *19*, 8900−8912.
(45) Ziessel, R.; Allen, B. D.; Rewinska, D. B.; Harriman, A. *Chem.—Eur. J.* **2009**, *15*, 7382−7393.
(46) Puntoriero, F.; Nastasi, F.; Campagna, S.; Bura, T.; Ziessel, R. *Chem.—Eur. J.* **2010**, *16*, 8832−8845.
(47) Shao, J.; Guo, H.; Ji, S.; Zhao, J. *Biosens. Bioelectron.* **2011**, *26*, 3012−3017.
(48) Quartarolo, A. D.; Russo, N.; Sicilia, E. *Chem.—Eur. J.* **2006**, *12*, 6797−6803.
(49) Kand, D.; Kumar Mishra, P.; Saha, T.; Lahiri, M.; Talukdar, P. *Analyst* **2012**, *137*, 3921−3924.
(50) Savarese, M.; Aliberti, A.; De Santo, I.; Battista, E.; Causa, F.; Netti, P. A.; Rega, N. *J. Phys. Chem. A* **2012**, *116*, 7491−7497.
(51) Setiawan, D.; Kazaryan, A.; Martoprawiro, M. A.; Filatov, M. *Phys. Chem. Chem. Phys.* **2010**, *12*, 11238−11244.
(52) Hanson, K.; Tamayo, A.; Diev, V. V.; Whited, M. T.; Djurovich, P. I.; Thompson, M. E. *Inorg. Chem.* **2010**, *49*, 6077−6084.
(53) Takizawa, S.-y.; Aboshi, R.; Murata, S. *Photochem. Photobiol. Sci.* **2011**, *10*, 895−903.
(54) Frisch, M. J.; Trucks, G. W.; Schlegel, H. B.; Scuseria, G. E.; Robb, M. A.; Cheeseman, J. R.; Scalmani, G.; Barone, V.; Mennucci, B.; Petersson, G. A.; Nakatsuji, H.; Caricato, M.; Li, X.; Hratchian, H. P.; Izmaylov, A. F.; Bloino, J.; Zheng, G.; Sonnenberg, J. L.; Hada, M.; Ehara, M.; Toyota, K.; Fukuda, R.; Hasegawa, J.; Ishida, M.; Nakajima, T.; Honda, Y.; Kitao, O.; Nakai, H.; Vreven, T.; Montgomery, J. A., Jr.; Peralta, J. E.; Ogliaro, F.; Bearpark, M.; Heyd, J. J.; Brothers, E.; Kudin, K. N.; Staroverov, V. N.; Kobayashi, R.; Normand, J.; Raghavachari, K.; Rendell, A.; Burant, J. C.; Iyengar, S. S.; Tomasi, J.; Cossi, M.; Rega, N.; Millam, J. M.; Klene, M.; Knox, J. E.; Cross, J. B.; Bakken, V.; Adamo, C.; Jaramillo, J.; Gomperts, R.; Stratmann, R. E.; Yazyev, O.; Austin, A. J.; Cammi, R.; Pomelli, C.; Ochterski, J. W.; Martin, R. L.; Morokuma, K.; Zakrzewski, V. G.; Voth, G. A.; Salvador, P.; Dannenberg, J. J.; Dapprich, S.; Daniels, A. D.; Farkas, Ö.; Foresman, J. B.; Ortiz, J. V.; Cioslowski, J.; Fox, D. J. *Gaussian 09W* (Revision A.1), Gaussian Inc.: Wallingford, CT, 2009.